Photonic Crystal Fiber for Efficient Raman Scattering of CdTe Quantum Dots in Aqueous Solution

Jacky S. W. Mak, Abdiaziz A. Farah, Feifan Chen, and Amr S. Helmy*

The Edward S. Rogers Sr. Department of Electrical and Computer Engineering, University of Toronto, 10 King's College Road, Toronto, Ontario, M5S 3G4 Canada.

ABSTRACT A novel hollow-core photonic crystal fiber platform was used for the first time to observe clear vibrational modes of the CdTe core, $CdS_{0.7}Te_{0.3}$ interface, and carboxylate-metal complexes in dilute aqueous CdTe quantum dot (QD) solutions. These modes demonstrate the presence of crystalline cores, defects, and surface passivation responsible for photoluminescent efficiency and stability. In addition, 3-mercaptopropionic acid (MPA)-capped QDs show higher crystallinity and stability than those capped with thioglycolic acid (TGA) and 1−thioglycerol (TG). This detailed, nondestructive characterization was carried out using Raman spectroscopy for solutions with QD concentration of 2 mg/mL, which is similar to their concentration during synthesis process. This platform can be extended to the *in situ* studies of any colloidal nanoparticles and aqueous solutions of relevant biological samples using Raman spectroscopy.

KEYWORDS: photonic crystal fiber · thiol-capped quantum dots · Raman spectroscopy · thioglycolic acid · 3-mercaptopropionic acid · 1−thioglycerol

Colloidal quantum dots (QDs) are suspensions of semiconductor nanoparticles that offer both the intriguing optical properties of quantum-confined particles, and the practical advantages of solution-based processing.[1−3] In the past two decades, aqueous synthesis of colloidal QDs has gained much popularity and evolved tremedously.[4−8] This simple and cost-effective technique allows very small (2−6 nm), monodisperse, and highly water-soluble QDs to be synthesized in gram quantities. QD capping plays a pivotal role in the properties and utility of the material; the use of short-chain thiols, such as thioglycolic acid (TGA), as capping agents has been shown to greatly improve the photoluminescent (PL) quantum efficiency of as-synthesized QDs to values of 40−60%.[4] 3-Mercaptopropionic acid (MPA) has also shown to offer a larger range of size and PL tunability and a longer emission decay time.[4] Other thiols, such as 1−thioglycerol (TG), are found to be more suitable for synthesizing stable core−shell QDs.[7] The unique properties of the different colloidal QDs have potentials for a wide field of novel applications ranging from photovoltaics[9] and optoelectronics,[10] to biosensing,[11] bioimaging,[12] and even cancer treatments.[13]

One of the most important technological challenges in QD advancement is the development of a cost-effective, reliable, and sensitive optical monitoring system to control the physical, chemical, and size-dependent properties of QDs before, during, and after their fabrication on a nanometer scale. To measure and compare these properties between the different QDs, many analytical techniques have been employed including but not limited to PL, electroluminescence (EL), ultraviolet−visible spectroscopy (UV−vis), transmission electron microscope (TEM) or high resolution transmission electron microscope (HRTEM), capillary zone electrophoresis (CZE), X-ray diffraction (XRD), and X-ray photoelectron spectroscopy (XPS). These techniques provide valuable information on the composition and properties of the QDs; yet, none of them describes how the capping agents interact with the core of the QDs. Their impact on the overall molecular structure, molecular complex, and different QD properties also remains unclear. Consequently, this limits our capability to improve the quantum efficiency, stability, and bioconjugating ability further from what has been achieved today. Complex QD designs for increasing performance and functionalities in different applications remain very challenging.

Fourier-transform infrared spectroscopy (FT-IR) can be an alternative for determining the molecular interactions between the QDs and their capping agents. However, the strong and broad absorption bands of water often overlap with those from the QDs and stabilizing agents. This limits the number of vibrational modes that can be resolved.

A complementary technique to FT-IR is Raman spectroscopy, which is a rapid and nondestructive means of probing molecular vibrations optically through inelastic

* Address correspondence to a.helmy@utoronto.ca.

Received for review January 14, 2011 and accepted April 25, 2011.

Published online April 25, 2011
10.1021/nn200157z

scattering. Raman provides the unique vibrational modes or "fingerprints" of the molecules that enable similar molecular structures to be unambiguously distinguished and identified. More importantly, the vibrational modes of water are inherently weaker in Raman scattering than in FT-IR. Distinctive Raman modes of colloidal QDs in their native and dilute aqueous environment can be readily obtained without significant interference. However, Raman scattering has not been successful in characterizing QDs because it is generally very weak compared to elastic scattering, and it is further weakened in aqueous or dilute solutions; therefore, it has only been used in characterizing QDs coated on films or in powder form.[8,14−17] Surface-enhanced Raman spectroscopy (SERS) has also been used to obtain an enhanced Raman signal from solutions.[18−20] However, metallic nanoparticles have to be mixed with the QD solution, which could alter the structure and properties of the QDs from its as-synthesized state due to conformational changes when interacting with metallic nanoparticles.

An alternative means of enhancing Raman signals from aqueous or diluted solutions, without the need of additional metallic nanoparticles, is hollow-core photonic crystal fiber (HC-PCF).[21,22] HC-PCFs are optical fibers consisting of a central air core and a high air-filling fraction cladding formed by a periodic air hole array in silica. The periodic air holes confine the pump laser inside the central core of the PCF through both photonic bandgap effects and total internal reflections.[23] This is a distinguishing feature of our technique as we can utilize both guiding mechanisms by selectively filling the central air core with QD solution to maintain the photonic bandgap effects of the cladding. By confining both the pump laser and the solution along the length of the PCF, a larger volume for light−matter interaction is achieved compared to that of a conventional Raman spectroscopy scheme.[24,25] Figure 1 compares the conventional Raman spectroscopy scheme with the one using HC-PCF as an interaction medium for Raman spectroscopy. In conventional Raman spectroscopy (Figure 1a), the pump laser is focused directly into the QD solution to generate Raman scattering. Most of the Raman signal detected is scattered from the beam waist of the pump laser in which the pump laser is most intense. In this case, the pump laser and the QDs are only interacting in the volume limited by the spot size of the pump laser in the lateral direction and the depth of field in the axial direction. Since Raman signals are scattered in all directions, only a fraction of the scattered signal is collected by the objective and detected by the detector due to the limited numerical aperture of the objective. In the case of an aqueous QD solution, the amount of scattered signal detected from the small quantity of QDs dispersed in water is very minimal.

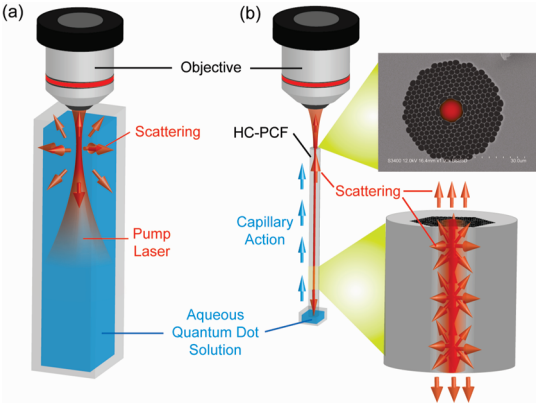

Figure 1. Raman scattering and signal collection in (a) conventional Raman spectroscopy and (b) Raman spectroscopy using HC-PCF.

By employing HC-PCF as the medium for light−matter interactions (Figure 1b), both the pump laser and the QD solution can be confined within the central core of the HC-PCF. Subsequently, the confined laser power within the core induces a strong interaction with the solution that is filled inside. Thus, Raman signals are scattered throughout the whole length of the fiber as opposed to just the depth of field of the objective in the conventional scheme. Since Raman signals are only slightly shifted from the wavelength of the pump laser, they will also be confined inside the central core of the PCF. As a result, the output signal from the fiber end will be collected more efficiently by the objective and directed to the detector. In addition, it is important to note that the pump laser is confined inside the "liquid" core of the PCF; thus, the interaction between the pump laser and the glass wall of the fiber is minimal and the resulted interference is very limited in the presence of other vibrational modes and backgrounds. With the use of HC-PCF, the detected Raman signal can be 2 orders of magnitude greater than that of the conventional Raman spectroscopy.[26] In addition, the unprecedented interaction volume can be increased by extending the length of the fiber. The limiting factors are the absorption and the attenuation due to propagation loss of the pump laser inside the central core, which we can optimize through appropriate designs of the HC-PCF.

In the essence of combining HC-PCF with Raman spectroscopy, the practical advantages of optical fibers are added to the conventional scheme. This includes the high flexibility and compactness of optical fibers for remote sensing and *in situ* detections, sampling versatility, and potential for low-cost analysis as the cost of HC-PCF drops dramatically through economies of scale. In addition, HC-PCF requires only a very small sample volume for detection, and it is capable of detecting multiple compounds in parallel. This is crucial in many biological, environmental, and forensic

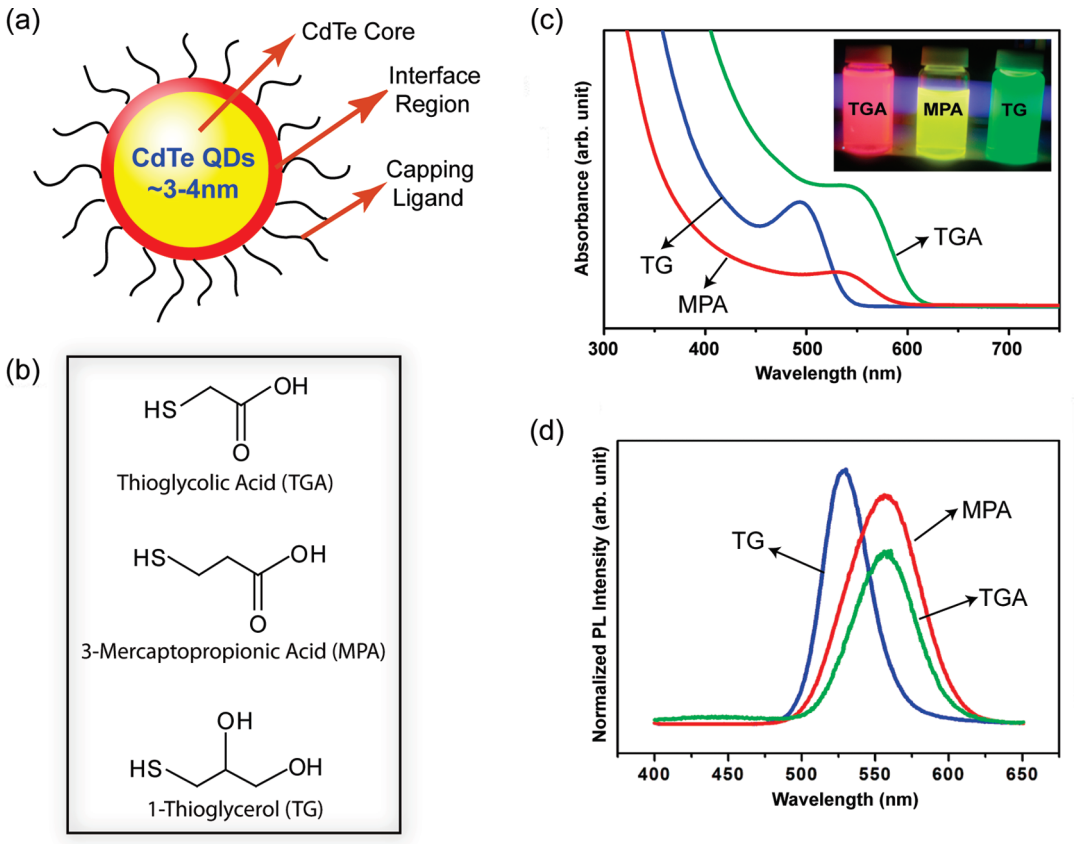

Figure 2. (a) Core−shell structure of CdTe QDs. (b) Molecular structure of capping ligands. (c) UV−vis spectra of the CdTe QDs (inset: fluorescent images of the QD solutions). (d) PL profile of the QDs.

applications where sample analysis with only nanoliter volume is required.

In nanomaterial analysis, this platform shows potential for low-cost *in situ* monitoring of QD structure during the synthesis process. The usefulness of HC-PCF for Raman spectroscopy has recently been demonstrated in the studies of ZnO nanoparticles synthesized through the base hydrolysis method,[21] and colloidal CdTe nanoparticles postsynthesized using rapid thermal annealing.[22] In these studies, Raman modes of the ZnO and CdTe nanoparticles were obtained owing to the detected signal enhancement provided by the HC-PCF.

In this study, we report the enhanced detected Raman signals from aqueous solutions of thiol-stabilized CdTe QDs through the use of HC-PCF. The structure of the highly fluorescent CdTe QDs and the three different ligands used for stabilization are shown in Figure 2 along with their UV−vis and PL profile. Strong and clear vibrational modes ascribed to the CdTe semiconductor core, capping agents, and their interface were obtained for the first time in the aqueous medium. The observed Raman vibrational modes are divided into three regimes. The modes in the low Raman shift regime reveal the low crystallinity of CdTe QDs capped with TGA due to a large inclusion of Te compounds and surface defects. The modes in the mid and high Raman shift regime reveal the formation of thiolates, and Cd−S bonds between the thiolate and the CdTe core, which stabilize the QD through a structured CdS_xTe_{1-x} ternary compound. MPA is also found to promote the formation of unidentate and chelating bidentate complexes with the CdTe core. These complexes further passivate the QD and potentially improve its stability at the expense of its solubility and bioconjugating ability. This work substantiates the promise of HC-PCF in enhancing the Raman scattering signal of nanoparticles in aqueous solutions and enables possible studies of molecular structures relating to the different properties of QDs.

RESULTS AND DISCUSSION

Figure 3 shows the Raman spectra of aqueous CdTe QDs from 100 to 1750 cm^{-1}. The spectra are divided into three regimes in which the peaks are correlated to the vibrational modes in the CdTe semiconductor core, capping ligands, and their interfacial structures. Some of the modes are broad because they overlap with multiple weak Raman modes that are located in proximity. These modes may originate from different functional groups, different conformations of the same functional groups, or both. The limited sensitivity of the system prevented them from being resolved.

CdTe Core and Te Defects. In the low Raman shift regime, between 100 and 200 cm^{-1} as depicted in Figure 3(a), Raman modes corresponding to the crystalline core and

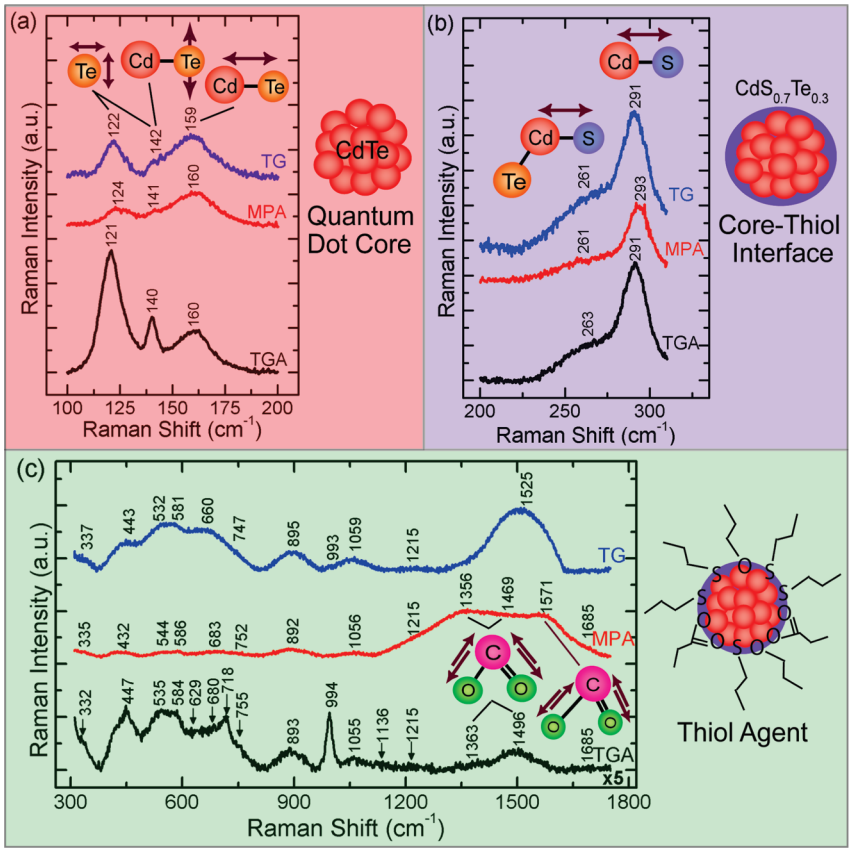

Figure 3. Raman spectra of thiol-capped CdTe QDs dispersed in aqueous solutions. The Raman shift between (a) 100−200, (b) 200−310, and (c) 310−1750 cm^{-1} correspond to the low, medium, and high Raman shift regimes in which Raman modes of the QD core (red box), core-thiol interface (purple box), and thiol agents (green box) are observed respectively. Te defect, CdTe LO, and CdTe TO modes of the QD core are shown graphically in panel a. CdS and $CdS_{0.7}Te_{0.3}$ modes of the core−thiol interface compound are shown in panel b. Carboxylate symmetric and asymmetric stretches of the thiol agents are shown in panel c. TGA spectrum between 310−1750 cm^{-1} has been scaled for clarity.

Te defects of the CdTe QDs are observed. The peaks at ~120, ~140 and ~160 cm^{-1} are attributed to the Te A_1, Te E and CdTe TO, and CdTe LO modes of the QDs, respectively.[27−31] These modes are observed in all three spectra indicating that both the crystalline CdTe core and Te defects are presented in the QDs regardless of the type and structure of the capping agent used. In particular, the CdTe LO modes are shifted to the lower wavenumber by ~10 cm^{-1} compared to the LO mode of bulk CdTe crystal reported at ~170 cm^{-1}.[28,32] These shifts indicate the presence of phonon localization due to quantum confinement effects, which suggests that the expected zero-dimensional CdTe structures are indeed in place. In addition, the similar shifts of the CdTe LO mode among the three spectra show that similar crystalline sizes are formed with the three different capping ligands used. Moving toward the lower Raman shifts at ~120 and ~140 cm^{-1}, two Te modes are observed in the three spectra. The two Te modes indicate the presence of Te crystals, either within the center of the QD or the surface defects at the boundary of the QDs.[30,31,33] QDs with surface defects are known to have lower crystallinity and introduce trap states which reduces the PL quantum efficiency.[34] However, the amount of Te inclusions or surface defects cannot be quantified from the spectra as the Raman cross sections of Te modes are 75 times larger than that of the crystalline CdTe modes.[31] Because of the close proximity and broadness of the Te E and CdTe TO vibrational mode at 140 cm^{-1}, precise contribution of the Te E modes from QDs with different caps cannot be determined from their spectra. Nevertheless, we can calculate the intensity ratios of the Te A_1 mode to CdTe LO mode to compare the crystallinity of these QDs. As shown in Table 1, the ratio is highest for TGA-capped QDs, followed by those for TG and then MPA. In our previous study, we have shown that an increase in the ratio indicates an increase in Te inclusion or surface defects relative to the amount of CdTe crystals formed in the QDs.[22] This suggests that crystallinity improved from TGA-capped QDs to TG-capped QDs and is greatest with MPA-capped QDs. The improved crystallinity contributes to a greater PL efficiency with fewer trap states that led to nonradiative processes; thus, a brighter QD is synthesized with MPA. Overall, both the crystalline CdTe core and defects are observed in QDs capped with TGA, MPA, and TG. However, different crystalline cores are obtained with MPA-capped QDs being the most crystalline among the three solutions.

TABLE 1. Intensity Ratios of the Te A_1 Mode to CdTe LO Mode for CdTe QDs Capped with Different Thiol Agents

intensity ratio	TGA	TG	MPA
Te A_1/CdTe LO	2.949	0.901	0.499

Core–Thiol Interface. In the mid-Raman shift regime, between 200 and 310 cm^{-1}, Raman modes are attributed to the interactions between the QD core and the thiol capping agents as shown in Figure 3b. The two peaks at ~291 and ~260 cm^{-1} shown in this regime are ascribed to the surface optical phonon (SO) mode of the CdS compound[14,35] and CdS-like LO phonon mode of the ternary CdS_xTe_{1-x} compound, respectively.[36,37] The presence of the two CdS related modes denotes the formation of CdS compounds on the surface of the QDs. This suggests that Cd ions on the surface of the QD core are bonded with the S ions in the thiol terminus of the capping agents for stabilization. This hypothesis is supported by the absence of the S–H stretching modes, in the range of 2560–2590 cm^{-1}, in all three spectra (not shown), which shows that S–H bonds in the thiol groups are broken and have then formed thiolates. These thiolates have possibly interacted with Cd ions and formed CdS compounds around the CdTe core. Several other studies have also proposed the same interaction between the thiol group and the core of the QDs.[8,38,39] Since no visible CdS LO mode at ~300 cm^{-1} is observed, a CdS shell has not formed around the CdTe cores in the three solutions. Instead, a CdS_xTe_{1-x} ternary structure might have formed around the CdTe core, which is commonly formed upon heating processes.[40,41] It is known that the position of CdS-like LO mode shifts from 305.6 (at $x = 1$) to 258.7 cm^{-1} (at $x = 0$) as S content decreases in CdS_xTe_{1-x} compounds.[36] Using the experimentally observed wavenumbers and their corresponding CdS_xTe_{1-x} alloy compositions from Fischer *et al.*,[36] a composition around $CdS_{0.7}Te_{0.3}$ is estimated for all three QD samples capped with the different thiol agents. The rich S content in the alloys indicate that many thiolates are coupled with the CdTe cores and formed a system close to the CdS shell. This strongly indicates that thiolates are strongly passivating the surface of the QDs and thereby preventing the CdTe core from exposing and interacting with the environment. Strong surface passivation also contributes to a greater PL efficiency through elimination of surface defect states.

It is important to note that both the CdS SO and the CdS-like LO modes are observed in all three spectra with the different capping agents used. The peak position of the two modes are similar among the three spectra, suggesting that the QD core interacts similarly with the three thiol agents, thus achieving the same alloy composition. Since the three thiol agents have different chain lengths, this suggests that the degree of surface passivation might be unrelated to the length of the thiol chain bonded to the QD surface. This is in agreement with the finding from Algar *et al.*, in which a reduction of nonradiative decay rate with increasing alkyl thiol chain length was not observed; thus, there was no improvement on the surface passivation of the QDs with lengthy thiol agents.[42,43] In fact, it was suggested that the longer alkyl thiol chain of MPA and TG excludes water from the QD surface, resulting in a higher quantum yield than the ones capped with TGA (Figure 2d). Previously, it was reported that photo-oxidation of the surface thiol agents could catalyze the formation of disulfides through breaking the Cd–S bonds and reacting with a neighboring thiol group.[44,45] However, no S–S vibrational modes in the region between 480 and 510 cm^{-1} were observed in any of the three spectra. This indicates the absence of disulfide bonds and confirms that photo-oxidization has not occurred in our solutions. The strong surface passivation and the absence of photo-oxidization observed from the Raman spectra further demonstrate that the CdTe QDs capped with TGA, MPA, and TG are all highly stable in their native aqueous environment.

Carboxylate–Metal Complexes. In the high Raman shift regime, between 310 and 1750 cm^{-1}, vibrational modes of the thiol capping agents are observed as shown in Figure 3c. Notably, the peaks between 1330 and 1500 cm^{-1} and between 1570 and 1580 cm^{-1} are attributed to the symmetric and asymmetric stretching modes of the carboxylates, respectively.[8,39,46] These modes are only observed in TGA, and MPA-capped QDs, in which one end of the thiol chain is terminated with a carboxylic acid group. These modes indicate that the carboxylic acid groups are absorbed onto the QD surfaces as carboxylates, most likely by forming bonds with the Cd ions on the CdTe core. Though one-phonon Raman modes of CdO are not allowed due to the selection rules, no well-defined vibrational modes can be extracted from the Raman spectra.[47] Nevertheless, it is known that the carboxylic acid group can be absorbed on metals as carboxylates after deprotonation.[8,39,48,49] Multiple shifted modes of carboxylate symmetric stretches might also have risen if multiple complexes of the carboxylate would have been formed. As such, the two symmetric stretching modes observed are a result of two carboxylate–metal formations.

On the basis of previous work, carboxylate ions may coordinate to a metal in one of the three modes: unidentate, bridging bidentate, and chelating bidentate.[46,48] These complexes can be identified through the wavenumber separations, Δ, between the symmetric and asymmetric stretches of the carboxylate. Unidentate complexes exhibit Δ values (200–470 cm^{-1}) that are much greater than the ionic complexes. Conversely, chelating bidentate complexes exhibit Δ values (<110 cm^{-1}) that are much

TABLE 2. The Wavenumber Separations, Δ, between the Symmetric and Asymmetric Stretching Modes of the Carboxylate, and Their Corresponding Carboxylate–Metal

capping agent	separation between $\nu_s(COO)^a$ and $\nu_{as}(COO)$, Δ_1	structure	separation between $\nu_s(COO)^b$ and $\nu_{as}(COO)$, Δ_2	structure
TGA	187 cm^{-1}	bridging bidentate	70 cm^{-1}	chelating bidentate
MPA	215 cm^{-1}	unidentate	102 cm^{-1}	chelating bidentate

[a] Symmetric stretches between 1300 and 1400 cm^{-1}. [b] Symmetric stretches between 1400 and 1500 cm^{-1}.

TABLE 3. Intensity Ratios of the Symmetric Carboxylate Stretch to CdS 2SO Mode

	intensity ratio	
capping agent	$\nu_s(COO)^a$/CdS 2SO	$\nu_s(COO)^b$/CdS 2SO
TGA	0.205	0.547
MPA	12.803	5.390

[a] Symmetric stretches between 1300 and 1400 cm^{-1}. [b] Symmetric stretches between 1400 and 1500 cm^{-1}.

less than the ionic complexes. Bridging bidentate complexes exhibit Δ values (140–190 cm^{-1}) that lie in between the chelating bidentate and ionic complexes. As shown in Table 2, both TGA and MPA-capped QDs have two carboxylate–metal complexes. Both TGA and MPA show the formation of chelating bidentate complexes. In addition, TGA formed the bridging bidentate complexes while MPA formed the unidentate complexes. It was recently reported that the carboxylate–metal complex changes from unidentate to bridging bidentate when the average size of the QDs increases from 8 to 20 nm.[8] However, the average particle sizes of our TGA and MPA-capped QDs calculated are very similar (*i.e.*, 3.20 nm for TGA-capped QDs and 3.07 nm for MPA-capped QDs using their first absorption maximum at 546 and 536 nm, respectively).[50] The small size difference between the two QD solutions is unlikely to cause a difference in the carboxylate–metal complex. This suggests that the length of the alkyl thiol chain might have influenced not only the type of complexes formed but also the amount of complexes formed. To compare the quantity of carboxylate–metal complex formed between the different interactions and QD solutions, the intensity ratios of the COO symmetric stretches to the CdS 2SO mode are calculated. As shown in Table 3, the two ratios are much greater than 1 for MPA-capped QDs and less than 1 for TGA-capped QDs. The large ratio implies that a large quantity of carboxylate ions is coordinated with the Cd ions. This is not only suggesting that the formation of carboxylate–metal complexes is much more favorable with MPA than with TGA, but also that the surface of the QD is more passivated by carboxylates in the MPA chain.[51,52] As a result, fewer defect sites are present in MPA-capped QDs, which corresponds to a higher PL quantum efficiency, however, in the sacrifice of losing its solubility potentially due to the reduction of free carboxylate ions. Bioconjugation to the QDs might also be limited with a reduced number of thiol terminuses on its surface. Since the chelating bidentate interactions of the carboxylates–metal complex are stronger than the unidentate interactions of the thiolates–metal complex, the larger quantity of chelating bidentate complexes formed in MPA-capped makes it more stable than the TGA-capped ones. Altogether, both TGA and MPA-capped QDs form carboxylate–metal complexes with the CdTe core, but the longer alkyl chain in MPA enabled a larger quantity of the complexes to be formed with it rather than with TGA; thus potentially permitting a higher stabilized QD to be synthesized with MPA.

CONCLUSION

In summary, we demonstrated the use of HC-PCF to obtain efficient Raman scattering of the different thiol-capped CdTe QDs in aqueous environment. Strong and clear Raman modes of the CdTe semiconductor core, capping ligands, and their interfacial structures were successfully observed and compared without integrating any metallic nanoparticles for enhancement. To the best of our knowledge, this is the first time that such strong Raman modes of the thiol-capped CdTe QDs in aqueous solution have been reported. The enhanced detected Raman signals were achieved through increased light–matter interaction and efficient accumulation of the Raman scattering signal along the whole length of the HC-PCF.

In addition, our experimental results also demonstrated the great potential of HC-PCF for optical sensing with minuscule analyte volume. The use of HC-PCF can be extended to the *in situ* studies of colloidal nanoparticles using Raman spectroscopy. Physical changes of the QD structure, such as crystallinity, interfacial modes, and surface passivation, can be monitored and controlled dynamically during the various synthesis processes for property optimizations. For example, surface chemistry between QDs and electrode surface can be optimized to achieve efficient sensitized photocurrents for practical photovoltaic devices. Furthermore, structural dynamics of the QDs can be determined experimentally in different biological systems to reveal the possible cause of some undesirable effects

(*i.e.*, cytotoxicity and photobleaching). Systematic study of molecular structures will enable us to better understand the basis of different QD properties which further optimizes our QD designs for different applications. Ultimately, HC-PCF can be served as a platform for studying the vibrational modes of complex aqueous solutions of relevant biological samples such as DNA.[53]

METHODS AND MATERIALS

The thiol-capped CdTe quantum dots (QDs) used in this study were synthesized with minor modification to literature procedure.[54,55] Sodium borohydride ($NaBH_4$, 99%), tellurium powder (~200 mesh, 99.8%), cadmium chloride ($CdCl_2$, 99%), thioglycolic acid (TGA) (98%), 3-mercaptopropionic acid (MPA) (99%), and 1-thioglycerol (TG) (99%) purchased from Aldrich chemicals. All chemicals were used as received; Millipore Q water (18 sm) were used throughout the nanocrystal synthesis.

Synthesis of TGA-capped CdTe QDs: 300 mg (7.90 mmol) of $NaBH_4$ was dissolved in 10 mL of water under argon environment and cooled in an ice bath. A 400 mg (3.14 mmol) portion of tellurium powder was added, and the reaction mixture was left stirring for 2 h to get a deep pink-purple clear solution. The resulting NaHTe solution was kept under argon before use. $CdCl_2$ (1.15 g, 6.28 mmol) was then dissolved in 70 mL of Millipore water and bubbled with argon for 20 min. One mL (15.08 mmol) of TGA was slowly added to this solution, which results in the formation of white precipitate due to the formation of Cd−TGA complex in the solution. The pH value of the solution was adjusted to 11.0 by dropwise addition of 2.0 M NaOH solution with stirring. The freshly prepared NaHTe solution was then rapidly added to the Cd precursor solution at room temperature. After being continuously stirred at room temperature for 10 min, the resulting orange solution is refluxed for a predetermined time (2−16 h) and then cooled to room temperature. The obtained CdTe NCs were precipitated by the addition of reagent grade acetone and were isolated and purified by repeated precipitation/centrifugation cycles with acetone/water and dried in vacuum for overnight. Solid CdTe QD samples were then weighted and dispersed in deionized water to prepare aqueous solutions of 2 mg/mL and 0.4 mg/mL for Raman and photoluminescence (PL) measurements respectively.

MPA-capped CdTe QDs were obtained using 400 mg of tellurium powder, 297 mg of $NaBH_4$, 1.15 g of $CdCl_2$, and 1.15 mL of MPA as described above. TG-capped CdTe QDs were obtained using 565 mg of tellurium powder, 420 mg of $NaBH_4$, 1.0 g of $CdCl_2$ and 1.62 mL of TG as described above.

Raman spectra were acquired using a Horiba Jobin Yvon HR800 micro-Raman system equipped with a CW 632.8 nm HeNe laser in the range of 2−5 mW. The spectral resolution of the spectrometer was about 1 cm^{-1}. The laser light was focused onto the hollow-core photonic crystal fibers (HC-PCFs) using a 100× objective. Each spectrum was averaged over 40 measurements with an accumulation time of 30 s. Room temperature PL measurements were performed using a Perkin-Elmer luminescence spectrophotometer in aqueous solution. The HC-PCFs used in these experiments were obtained from NKT Photonics, HC-800-01. Each piece was segmented, stripped, and cleaved into pieces of ~6 cm long. The core of the HC-PCF was selectively filled, using a technique developed by Irizar *et al.*,[21] to allow enhancement of the detected Raman signal through bandgap confinement of the pump laser. Raman spectra obtained were baseline removed and fitted with Gaussian or Gaussian−Lorentzian mixed functions to determine their peak positions, amplitudes, and full-width at half-maxima (FWHMs). The positions of the functions fit to the spectra are labeled in Figure 3.

Acknowledgment. We thank the Natural Sciences and Engineering Research Council of Canada (NSERC) for financial support.

Supporting Information Available: Summary of Raman peaks obtained from TGA, MPA, and TG-capped CdTe QDs, and their proposed assignments; CdTe QD spectra fit with Gaussian and Gaussian−Lorentzian mixed functions; spectra comparison of water, TG, and diluted TG; and Raman spectra of TGA, MPA, and TG. This material is available free of charge *via* the Internet at http://pubs.acs.org.

REFERENCES AND NOTES

1. Medintz, I. L.; Uyeda, H. T.; Goldman, E. R.; Mattoussi, H. Quantum Dot Bioconjugates for Imaging, Labelling and Sensing. *Nat. Mater.* **2005**, *4*, 435–446.
2. Wood, V.; Bulović, V. Colloidal Quantum Dot Light-Emitting Devices. *Nano Rev.* **2010**, *1*, 5202–5209.
3. Sargent, E. H. Infrared Photovoltaics Made by Solution Processing. *Nat. Photon.* **2009**, *3*, 325–331.
4. Rogach, A. L.; Franzl, T.; Klar, T. A.; Feldmann, J.; Gaponik, N.; Lesnyak, V.; Shavel, A.; Eychmüller, A.; Rakovich, Y. P.; Donegan, J. F. Aqueous Synthesis of Thiol-Capped CdTe Nanocrystals: State-of-the-Art. *J. Phys. Chem. C* **2007**, *111*, 14628–14637.
5. Zhang, H.; Sun, P.; Liu, C.; Gao, H.; Xu, L.; Fang, J.; Wang, M.; Liu, J.; Xu, S., L-Cysteine Capped CdTe-CdS Core-Shell Quantum Dots: Preparation, Characterization and Immuno-Labeling of HeLa Cells. *Luminescence* [Online early access] doi: 10.1002/bio. Published online December 16, 2009; http://onlinelibrary.wiley.com/doi/10.1002/bio.1188/pdf (accessed Jul 28, 2010).
6. Liu, J.; Shi, Z.; Yu, Y.; Yang, R.; Zuo, S., Water-Soluble Multicolored Fluorescent CdTe Quantum Dots: Synthesis and Application for Fingerprint Developing. *J. Colloid Interface Sci.* 2010, *342*, 278−282; Epub 2009 Oct 29.
7. Wang, C.; Zhang, H.; Zhang, J.; Li, M.; Sun, H.; Yang, B. Application of Ultrasonic Irradiation in Aqueous Synthesis of Highly Fluorescent CdTe/CdS Core−Shell Nanocrystals. *J. Phys. Chem. C* **2007**, *111*, 2465–2469.
8. Abd El-sadek, M. S.; Ram Kumar, J.; Moorthy Babu, S. The Role of Potassium Tellurite as Tellurium Source in Mercaptoacetic Acid-Capped CdTe Nanoparticles. *Curr. Appl. Phys.* **2010**, *10*, 317–322.
9. Sargent, E. H. Solar Cells, Photodetectors, and Optical Sources from Infrared Colloidal Quantum Dots. *Adv. Mater.* **2008**, *20*, 3958–3964.
10. Cho, K.-S.; Lee, E. K.; Joo, W.-J.; Jang, E.; Kim, T.-H.; Lee, S. J.; Kwon, S.-J.; Han, J. Y.; Kim, B.-K.; Choi, B. L.; *et al.* High-Performance Crosslinked Colloidal Quantum-Dot Light-Emitting Diodes. *Nat. Photon.* **2009**, *3*, 341–345.
11. Qian, X.; Peng, X.-H.; Ansari, D. O.; Yin-Goen, Q.; Chen, G. Z.; Shin, D. M.; Yang, L.; Young, A. N.; Wang, M. D.; Nie, S. *In Vivo* Tumor Targeting and Spectroscopic Detection with Surface-Enhanced Raman Nanoparticle Tags. *Nat. Biotechnol.* **2008**, *26*, 83–90.
12. Kim, S.; Lim, Y. T.; Soltesz, E. G.; De Grand, A. M.; Lee, J.; Nakayama, A.; Parker, J. A.; Mihaljevic, T.; Laurence, R. G.; Dor, D. M.; *et al.* Near-Infrared Fluorescent Type II Quantum Dots for Sentinel Lymph Node Mapping. *Nat. Biotechnol.* **2004**, *22*, 93–97.
13. Yaghini, E.; Seifalian, A. M.; MacRobert, A. J. Quantum Dots and Their Potential Biomedical Applications in Photosensitization for Photodynamic Therapy. *Nanomedicine* **2009**, *4*, 353–363.

14. Schreder, B.; Schmidt, T.; Ptatschek, V.; Spanhel, L.; Materny, A.; Kiefer, W. Raman Characterization of CdTe/CdS "Core-Shell" Clusters in Colloids and Films. *J. Cryst. Growth* **2000**, *214–215*, 782–786.
15. Byrne, S. J.; Corr, S. A.; Rakovich, T. Y.; Gun'ko, Y. K.; Rakovich, Y. P.; Donegan, J. F.; Mitchell, S.; Volkov, Y. Optimisation of the Synthesis and Modification of CdTe Quantum Dots for Enhanced Live Cell Imaging. *J. Mater. Chem.* **2006**, *16*, 2896–2902.
16. Zhang, J.-Y.; Wang, X.-Y.; Xiao, M.; Qu, L.; Peng, X. Lattice Contraction in Free-Standing CdSe Nanocrystals. *Appl. Phys. Lett.* **2002**, *81*, 2076–2078.
17. Baranov, A. V.; Rakovich, Y. P.; Donegan, J. F.; Perova, T. S.; Moore, R. A.; Talapin, D. V.; Rogach, A. L.; Masumoto, Y.; Nabiev, I. Effect of ZnS Shell Thickness on the Phonon Spectra in CdSe Quantum Dots. *Phys. Rev. B* **2003**, *68*, 165306.
18. Castro, J. L.; López-Ramírez, M. R.; Centeno, S. P.; Otero, J. C. Adsorption of Mercaptoacetic Acid on a Colloidal Silver Surface as Investigated by Raman Spectroscopy. *Biopolymers* **2004**, *74*, 141–145.
19. Castro, J. L.; López-Ramírez, M. R.; Arenas, J. F.; Otero, J. C. Surface-Enhanced Raman Scattering of 3-Mercaptopropionic Acid Adsorbed on a Colloidal Silver Surface. *J. Raman Spectrosc.* **2004**, *35*, 997–1000.
20. Wang, Y.; Zhang, J.; Jia, H.; Li, M.; Zeng, J.; Yang, B.; Zhao, B.; Xu, W.; Lombardi, J. R. Mercaptopyridine Surface-Functionalized CdTe Quantum Dots with Enhanced Raman Scattering Properties. *J. Phys. Chem. C* **2008**, *112*, 996–1000.
21. Irizar, J.; Dinglasan, J.; Goh, J. B.; Khetani, A.; Anis, H.; Anderson, D.; Goh, C.; Helmy, A. S. Raman Spectroscopy of Nanoparticles Using Hollow-Core Photonic Crystal Fibers. *IEEE J. Sel. Top. Quant.* **2008**, *14*, 1214–1222.
22. Rutledge, S. A.; Farah, A. A.; Dinglasan, J.; Anderson, D. J.; Das, A.; Goh, J.; Goh, C.; Helmy, A. S. Postsynthesis Crystallinity Improvement of Colloidal CdTe Nanoparticles Using Rapid Thermal Annealing. *J. Phys. Chem. C* **2009**, *113*, 20208–20213.
23. Fini, J. M. Microstructure Fibres for Optical Sensing in Gases and Liquids. *Meas. Sci. Technol.* **2004**, *15*, 1120.
24. Benabid, F.; Knight, J. C.; Antonopoulos, G.; Russell, P. St J. Stimulated Raman Scattering in Hydrogen-Filled Hollow-Core Photonic Crystal Fiber. *Science* **2002**, *298*, 399–402.
25. Yan, H.; Gu, C.; Yang, C.; Liu, J.; Jin, G.; Zhang, J.; Hou, L.; Yao, Y. Hollow Core Photonic Crystal Fiber Surface-Enhanced Raman Probe. *Appl. Phys. Lett.* **2006**, *89*, 204101-3.
26. Yang, X.; Shi, C.; Wheeler, D.; Newhouse, R.; Chen, B.; Zhang, J. Z.; Gu, C. High-Sensitivity Molecular Sensing using Hollow-Core Photonic Crystal Fiber and Surface-Enhanced Raman Scattering. *J. Opt. Soc. Am. A* **2010**, *27*, 977–984.
27. Ochoa, O. R.; Witkowski Iii, E. J.; Colajacomo, C.; Simmons, J. H.; Potter, B. G., Jr. Raman Characterization of CdTe Nanocrystallites Embedded in a Glass Matrix. *J. Mater. Sci. Lett.* **1997**, *16*, 613–616.
28. Vinogradov, V. S.; Karczewski, G.; Kucherenko, I. V.; Mel'nik, N. N.; Fernandez, P. Raman Spectra of Structures with CdTe-, ZnTe-, and CdSe-Based Quantum Dots and Their Relation to the Fabrication Technology. *Phys. Solid State* **2008**, *50*, 164–167.
29. Amirtharaj, P. M.; Pollak, F. H. Raman Scattering Study of the Properties and Removal of Excess Te on CdTe Surfaces. *Appl. Phys. Lett.* **1984**, *45*, 789–791.
30. Shin, S. H.; Bajaj, J.; Moudy, L. A.; Cheung, D. T. Characterization of Te Precipitates in CdTe Crystals. *Appl. Phys. Lett.* **1983**, *43*, 68–70.
31. Morell, G.; Reynés-Figueroa, A.; Katiyar, R. S.; Farías, M. H.; Espinoza-Beltran, F. J.; Zelaya-Angel, O.; Sánchez-Sinencio, F. Raman Spectroscopy of Oxygenated Amorphous CdTe Films. *J. Raman Spectrosc.* **1994**, *25*, 203–207.
32. Islam, S. S.; Rath, S.; Jain, K. P.; Abbi, S. C.; Julien, C.; Balkanski, M. Forbidden One-LO-Phonon Resonant Raman Scattering and Multiphonon Scattering in Pure CdTe Crystals. *Phys. Rev. B* **1992**, *46*, 4982.
33. Na, H.-K.; Shon, P.-K. A Raman Scattering Study of CdTe/p-(111)InSb Heterointerfaces Grown by R.F. Sputtering in High Vacuum. *Solid State Commun.* **1993**, *85*, 609–612.
34. Gilbert, B.; Huang, F.; Lin, Z.; Goodell, C.; Zhang, H.; Banfield, J. F. Surface Chemistry Controls Crystallinity of ZnS Nanoparticles. *Nano Lett.* **2006**, *6*, 605–610.
35. Schreder, B.; Schmidt, T.; Ptatschek, V.; Winkler, U.; Materny, A.; Umbach, E.; Lerch, M.; Muller, G.; Kiefer, W.; Spanhel, L. CdTe/CdS Clusters with "Core−Shell" Structure in Colloids and Films: The Path of Formation and Thermal Breakup. *J. Phys. Chem. B* **2000**, *104*, 1677–1685.
36. Fischer, A.; Anthony, L.; Compaan, A. D. Raman Analysis of Short-Range Clustering in Laser-Deposited CdS_xTe_{1-x} Films. *Appl. Phys. Lett.* **1998**, *72*, 2559–2561.
37. Pal, R.; Dutta, J.; Chaudhuri, S.; Pal, A. K. CdS_xTe_{1-x} Films: Preparation and Properties. *J. Phys. D: Appl. Phys.* **1993**, *26*, 704.
38. Kim, J. E.; Hwang, C.-S.; Yoon, S. Synthesis and Surface Characterization by Raman Spectroscopy of Water-Dispersible ZnS: Mn Nanocrystals Capped with Mercaptoacetic Acid. *Notes* **2008**, *29*, 1247.
39. Zhang, H.; Zhou, Z.; Yang, B.; Gao, M. The Influence of Carboxyl Groups on the Photoluminescence of Mercaptocarboxylic Acid-Stabilized CdTe Nanoparticles. *J. Phys. Chem. B* **2002**, *107*, 8–13.
40. Dhere, R.; Wu, X.; Albin, D.; Perkins, C.; Moutinho, H.; Gessert, T. Formation and Characterization of CdS_xTe_{1-x} Alloys Prepared from Thin Film Couples of CdS and CdTe. *IEEE PV Spec. Conf.* **2002**, 484–487.
41. Murali, K. R.; Palanisamy, T. Electrical and Optical Properties of Pulse Plated CdS_xTe_{1-x} Films. *Ionics* **2010**, *16*, 613–619.
42. Blum, A. S.; Moore, M. H.; Ratna, B. R. Quantum Dot Fluorescence as a Function of Alkyl Chain Length in Aqueous Environments. *Langmuir* **2008**, *24*, 9194–9197.
43. Aldeek, F.; Balan, L.; Lambert, J.; Schneider, R. The Influence of Capping Thioalkyl Acid on the Growth and Photoluminescence Efficiency of CdTe and CdSe Quantum Dots. *Nanotechnology* **2008**, *19*, 475401.
44. Kloepfer, J. A.; Bradforth, S. E.; Nadeau, J. L. Photophysical Properties of Biologically Compatible CdSe Quantum Dot Structures. *J. Phys. Chem. B* **2005**, *109*, 9996–10003.
45. Aldana, J.; Wang, Y. A.; Peng, X. Photochemical Instability of CdSe Nanocrystals Coated by Hydrophilic Thiols. *J. Am. Chem. Soc.* **2001**, *123*, 8844–8850.
46. Nakamoto, K. *Infrared and Raman Spectra of Inorganic and Coordination Compounds: Part B.*; Wiley: Hoboken, NJ, 2009.
47. Popović, Z. V.; Stanišić, G.; Stojanović, D.; Kostić, R. Infrared and Raman Spectra of CdO. *Phys. Status Solidi B* **1991**, *165*, K109–K112.
48. Socrates, G. *Infrared Characteristic Group Frequencies*; Wiley: New York, 1980.
49. Shevchenko, L. L. Infrared Spectra of Salts and Complexes of Carboxylic Acids and Some of Their Derivatives. *Russ. Chem. Rev.* **1963**, *32*, 201.
50. Yu, W. W.; Qu, L.; Guo, W.; Peng, X. Experimental Determination of the Extinction Coefficient of CdTe, CdSe, and CdS Nanocrystals. *Chem. Mater.* **2003**, *15*, 2854–2860.
51. Gao, M.; Kirstein, S.; Mohwald, H.; Rogach, A. L.; Kornowski, A.; Eychmuller, A.; Weller, H. Strongly Photoluminescent CdTe Nanocrystals by Proper Surface Modification. *J. Phys. Chem. B* **1998**, *102*, 8360–8363.
52. Zhang, H.; Wang, D.; Möhwald, H. Ligand-Selective Aqueous Synthesis of One-Dimensional CdTe Nanostructures. *Angew. Chem., Int. Ed.* **2006**, *45*, 748–751.
53. Abu-Ghazalah, R. M.; Irizar, J.; Helmy, A. S.; Macgregor, R. B., Jr. A Study of the Interactions that Stabilize DNA Frayed Wires. *Biophys. Chem.* **2010**, *147*, 123–129.
54. Klayman, D. L.; Griffin, T. S. Reaction of Selenium with Sodium Borohydride in Protic Solvents. A Facile Method for the Introduction of Selenium into Organic Molecules. *J. Am. Chem. Soc.* **1973**, *95*, 197–199.
55. Gu, Z.; Zou, L.; Fang, Z.; Zhu, W.; Zhong, X. One-Pot Synthesis of Highly Luminescent CdTe/CdS Core/Shell Nanocrystals in Aqueous Phase. *Nanotechnology* **2008**, *19*, 135604.